Magnetostrictive energy conversion ability of Iron Cobalt Vanadium alloy sheet: Experimental and theoretical evaluation

Borel Franck Toutsop Zangho, Yuanyuan Liu, Shurui Zhang, Mickaël Lallart, Laurent Morel, Gael Sebald, Pierre Tsafack, Benjamin Ducharne

Magnetostrictive energy conversion ability of Iron Cobalt Vanadium alloy sheet: Experimental and theoretical evaluation.

Toutsop Zangho Franck Borel[1,2,3], Yuanyuan Liu[3,4,5], Shurui Zhang[3,6,7], Mickaël Lallart[3], Laurent Morel[2], Gael Sebald[5], Pierre Tsafack[1], Benjamin Ducharne[3,5*]

[1] Faculty of Engineering and Technology, University of Buea, Buea, Cameroon.
[2] Univ. Lyon, Université Claude Bernard Lyon 1, INSA Lyon, Ecole Centrale de Lyon, CNRS, Ampère, UMR5005, 69622 Villeurbanne, France.
[3] Univ Lyon, INSA-Lyon, LGEF EA682, F69621, France.
[4] Space Structure Lab, Department of aerospace engineering, Tohoku University, Japan
[5] ELyTMaX IRL3757, CNRS, Univ. Lyon, INSA Lyon, Centrale Lyon, Université Claude Bernard Lyon 1, Tohoku University, Sendai, Japan.
[6] Institute of Fluid Science (IFS), Tohoku University, Sendai, Japan.
[7] Graduate School of Engineering, Tohoku University, Sendai, Japan.

* Corresponding author: benjamin.ducharne@insa-lyon.fr

Abstract

The increasing demand for autonomous devices has made the concept of energy harvesting a significant industrial and academic point of interest. In this domain, an ideal magnetostrictive material for converting mechanical vibrations into electrical energy in a cost-effective way (i.e., competing with the price of primary batteries) remains to be determined. Iron-Cobalt-Vanadium (Permendur, Co49-Fe49-V2) is a promising candidate: it is a soft ferromagnetic material with high magnetization saturation, high magnetostrictive coefficients, low price, and good availability.

In this study, the experimental magnetic characterization and simulation of Permendur sheets under tensile stress were performed, and their energy conversion capabilities were assessed. The conversion ability was predicted using thermodynamic Ericsson cycles from reconstructed anhysteretic curves. A maximum of 10.45 $mJ \cdot cm^{-3}$ energy density was obtained under a tensile stress of 480 MPa and a magnetic excitation of 5.5 $kA \cdot m^{-1}$. Then, an additional estimation was proposed to account for the hysteresis losses. For this, major hysteresis loops at different stress levels were considered, yielding an energy density of 3.52 $mJ \cdot cm^{-3}$. Finally, experimental Ericsson cycles were performed to prove the feasibility of the conversion and corroborate the energy level predictions.

Keywords: Magnetostriction, magnetostrictive materials, magneto-mechanical coupling, energy conversion, Ericsson cycle, hysteresis cycles.

I - Introduction

In the last two decades, the development of wireless and wearable devices has been remarkable. Recent developments in microelectronics with the low-power Very Large-Scale Integration (VLSI) design reduced the power consumption of wireless sensor networks to only tens of microwatts [1], yielding a proliferation of wirelessly connected devices and the development of the Internet of Things (IoT) [2]. Wireless sensors have reduced power requirements of hundreds of µW in Mica (class of wireless sensor nodes) with projections into tens of µW. The maximum power for most wireless nodes is typically 200 mW, which strongly depends on the sensor node's sampling rate, transmission range, and transmission speed [3]. The energy consumption of a self-powered device usually requires a few mJ to perform its operation (Scavenger Transmitter Module). According to [4] typical power demands for temperature sensors lie between 0.5-5mW, and 2-3 mW for acceleration sensors. Unfortunately, progress in energy storage and/or supply chains have not been as fast, and providing reliable and sustainable electrical energy to all of these systems remains a significant challenge. While conventional batteries, used in most applications, show limitations (e.g., low lifespan due to self-discharge, etc.), using ambient energy sources to obtain electrical energy constitutes an attractive alternative, which leads to the concept of "Energy Harvesting [5]."

A complete energy harvesting system includes three main parts: a conversion material (magnetostrictive, magnetocaloric, piezoelectric, thermoelectric, photovoltaic, etc.), a structure (mechanical, thermal, electromagnetic, etc.), and an electrical interface. All energy harvesting systems can be sorted according to the energy source and/or corresponding conversion material. Amongst typically available energy sources (solar, thermal, mechanical, etc.), mechanical

vibrations have many advantages, such as availability, energy levels that are compatible with the requirements of autonomous sensors, and ubiquity [6][7]. At a small scale (millimeters to centimeters), the preferred conversion mechanism remains to date piezoelectricity. More than 200 $mJ \cdot cm^3$ can be expected using piezoelectric material [8], which is larger than any other conversion method. Still, many drawbacks can be associated with the piezoelectric solution, including, in the first line, the absence in the market of large-volume specimens. Also, piezoelectric materials are fragile, exhibit a high output impedance, and can be degraded by aging and fatigue [9][10].

Magnetostrictive materials constitute a valid alternative: they are available in large quantities, they exhibit high allowable stress and high conversion properties (bidirectional conversion of energy in the elastic regimes, which is attractive as it does not degrade in time and provides almost instantaneous response [11]). Historically, magnetostrictive materials were initially exploited based on their ability to change shape under external magnetic fields [12]. But magnetostrictive energy harvesting utilizes the Villari effect (inverse effect) to convert strain into magnetic energy [13]. The conversion process in a magnetostrictive energy harvesting system can be done in 2 ways: by geometrically-induced reluctance change in the magnetic circuit [14][15] or by the direct magnetostrictive effect (Villari effect) [16]. Concerning the first method, it can be achieved by geometrical adjustment, including, for instance, varying the distance between the magnetostrictive material and a permanent magnet. This solution means to include an air gap to the magnetic circuit as a consequence of the resulting system losing its integrability; the role of magnetostriction may be secondary compared to the geometry change effect in this case. For the second method, i.e., systems using the magnetostrictive effect, two main

parameters are taken into consideration: the biasing magnetic field and the prestress; those parameters should be optimized according to the material's nature for maximal use of the Villari effect [17][18]. For this method, the prestress allows an increase in the stress value, implying the system to work around a functioning point.

Magnetostriction is a material property that causes material deformation when subjected to an external magnetic field [19-23]. Magnetostriction is associated with two magnetization mechanisms [24]:

- The domain wall motions
- The rotation of the magnetic moments within domains toward the field direction.

By definition, the Villari effect (also known as magneto-elastic coupling or inverse magnetostrictive coupling [13][25]) is the magneto-mechanical coupling corresponding to a change of magnetic flux density due to mechanical stress [13]. The magnetostrictive energy conversion principle is depicted in Fig. 1. When applying an external magnetic field, the active material converts electrical energy from mechanical vibration or tensile stress via magneto-mechanical coupling. More precisely, a wrapped coil converts the change in magnetic quantities associated with the magnetic and mechanical stimuli into electrical output through the Faraday law. Because of the bidirectional coupled nature of the problem, global optimization of the device is a complex process that necessitates encompassing the whole conversion scheme, starting from the energy conversion material that constitutes the core of the present study.

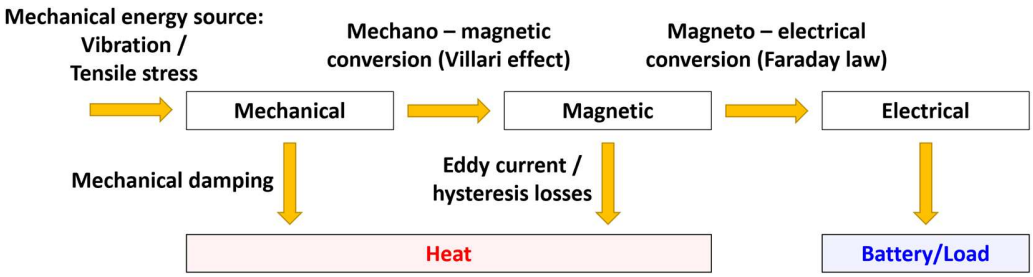

Fig. 1 – Illustration of the energy distribution in a magnetostrictive conversion system.

The amount of energy harvested by a magnetostrictive small-scale generator depends on the operating conditions (mechanical preload and magnetic bias) and design characteristics (amplitude and frequency of vibrations, device geometry, magnetic circuit, etc.). Several modeling tools were developed to analyze the influence of parameters on the harvester performances (energy conversion, etc.) [26]. Those include for instance:

- Mizukawa et al. in [9] described a model of a magnetostrictive energy harvester operating under a small-signal vibration excitation imposed over a constant prestress and magnetic bias using linearized constitutive equations.
- Palumbo et al. in [27] focused on the change of magnetostrictive properties under different mechanical prestresses and magnetic bias, and experimentally investigated the effect of parameter variations. The optimal operating condition and output power were obtained from these experiments. The obtained output power and induced voltage were interpolated by exponential fit.
- Davino et al. in [28] proposed a finite element method (FEM) Eddy current model for a magnetostrictive energy harvester, where the nonlinear static characteristic of the material is considered.

- Wang et al. in [29] proposed a vibration energy harvesting device using Metglas 2605SC and an alternative simulation technique.
- Park et al. in [30] designed vibrational harvesters that use both magnetostrictive and geometric reluctance variation effects. There, a magnetic bias field is provided by magnets to Galfenol alloy. During vibration stimulus, the distance variations between the sample and the magnet generate field changes and induce electromotive forces across the wrapping coils.
- Davino et al. in [31] conducted experiments on Galfenol energy harvesters considering various design parameters such as load resistance, beam thickness ratio, and bias magnetic field strength. The results proved that the harvesting loops in the B–H plane, are limited within the corresponding static magnetic characteristics extrema of the applied stress. This suggests the importance of the static characteristics to efficiently design the active material for harvesting purposes.
- Zucca et al. in [32] made a combined experimental and modeling approach and analyzed a transducer's behavior based on a Terfenol-D rod. They developed a bending-type energy harvester where a longitudinal force was applied at the head of the moving part of the beam.
- Yamaura et al. in [33] proposed an axial-type vibration energy harvester with an impact-sliding structure. A magnetostrictive rod is fixed magnetically, not mechanically. The rod vibrates longitudinally at its inherent frequency as free vibration excited by an impulsive force.
- Kita et al. in [34] have developed a unimorph-type Galfenol-based bending-type energy harvester. A maximum of 35% of conversion efficiency was achieved at an input frequency of 202 Hz.

- Liu et al. in [35] investigated the energy conversion abilities of Metglas 2605SA1 by performing experimental Ericsson cycles and through dedicated theoretical model predictions of the magnetic curves. Output magnetic energy densities between 0.1 and 1 mJ/cm3/cycle under stress values less than 100 MPa and magnetic excitation up to 4 kA/m.
- Berbyuk et al. in [36] developed a Galfenol-based energy harvester in axial mode and achieved 338 mW/cm3 power density. Based on experiments, it was found that for a given vibration frequency there is an optimal value of magnetic bias and mechanical pre-stress which maximize generated voltage and harvested power. Under optimized operational conditions and external excitations with frequency 50Hz the designed system generated about 10 V and harvests about 0.45 W power. Within the running conditions, the Galfenol rod power density was estimated to 340mW/cm3.

Understanding all the conversion stages involved in the energy harvesting process and their interactions starts with the proper selection and knowledge of the magnetostrictive material. The problem of the behavior of magnetostrictive materials concerns two points:

- The exact effect of mechanical stress on magnetic behavior: applying a mechanical stimulus modifies the material's microstructure and changes the magnetic properties. In the case of soft ferromagnetic materials, this change induces an increase in magnetic losses and a drop in efficiency.
- The highly nonlinear response of magnetostrictive materials: most studies consider the magnetostrictive material operating up to the middle range of magnetic excitation (linear behavior). This consideration strongly limits the application potentials and assessment of the performance of the associated energy harvester.

Even if a vast family of magnetostrictive materials exists, most energy harvesting systems described in the scientific literature rely on giant magnetostriction materials like Terfenol-D and Galfenol [37-41] (Table 1). But these materials are extremely costly (Table 1, right column), and a large-scale development for such energy harvesters would be a financial oddity. Other materials like Iron-Cobalt-Vanadium (Permendur, Co49-Fe49-V2) show high magnetostrictive activity and much lower prices (Table 1) but have never really been tested in an energy harvesting context.

Table 1: Characteristics of the magnetostrictive materials for energy harvesting

Material	Magnetostriction coefficient $\boldsymbol{\lambda_s}$ **(ppm)**	Magnetization saturation $\mathbf{P_s}$ **(T)**	Energy density at the material scale $\mathbf{W_{mat}}$ **($\mu J \cdot cm^{-3}$)**	Mechanical Preload $\boldsymbol{\sigma}$ **(MPa)**	Magnetic Bias	**Price**
Galfenol	400-500 [42]	1.75 [43]	49 [44]	No preload	1.1T [42]	10 $/g
Terfenol-D	1500-2000 [42]	1 [45]	40.7 [42]	6MPa	1.2T [42]	15 $/g
Permendur	80 [42]	2.35 [46]	*Purpose of the present study*	No preload	5.5kA/m	0.1 $/g

Following these last observations and that most recently related works mainly focus on evaluating the overall performance of the magnetostrictive energy harvesting system without exploring the potential energy conversion performance at a material level, this paper aims at assessing the energy harvesting capability of Permendur laminated sheets. The magnetic behavior under tensile stress in the elastic range will be measured. Next, based on these experimental measurements, a simulation method of the anhysteretic behavior will be proposed and used to assess the potential energy conversion under tensile stress and magnetic excitation.

Then, another estimation of the converted energy density will be described to account for the hysteresis losses. Finally, experimental Ericsson energy cycles will be measured to prove the feasibility of the conversion process and validate Permendur as a relevant material for energy conversion applications.

The paper is organized as follows: Section 2 will present the experimental setup and some preliminary magneto-mechanical characterizations. These experimental observations will be simulated and discussed in Section 3. Section 4 will introduce the estimation methods for the converted energy. Section 5 will provide experimental Ericsson cycle proof of concept and will be followed by a general conclusion on the applicability of Permendur as energy harvesting material.

II – Experimental characterization

2.1) Experimental setup

Permendur has a high yield strength (σ_c = 1000 MPa) and a quasi-isotropic magnetic behavior in the sheet plane in no-stress conditions. Its low magnetocrystalline anisotropy induces no naturally preferred crystallographic orientation [47-49]. All tested specimens were extracted from the same batch. Dog-bone shape samples (Fig. 2) were cut by electrical discharge machining to avoid residual stress associated with the cutting process.

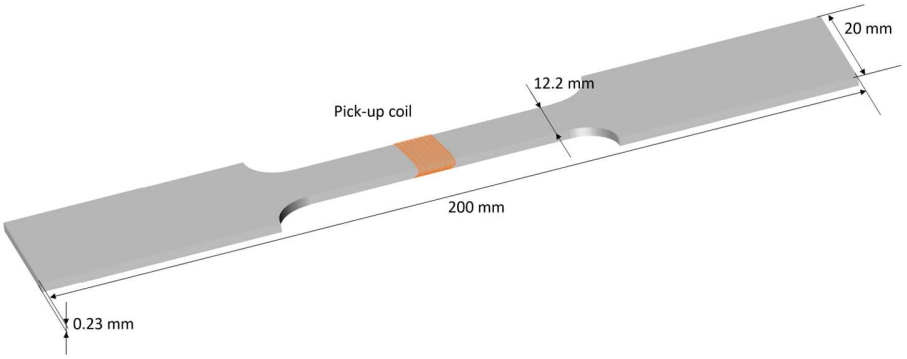

Fig. 2 – Permendur's dog-bone shape specimen dimensions

The experimental setup consisted of a traction-compression bench (Shimadzu AGS-X series) for the stress application. The magnetic inductor comprised two U-shaped electrical steel yokes (Grain-oriented Fe-3%Si). The legs' cross-section was 12 × 12 mm^2, and the inner distance between the legs was 30 mm. A 350-turns excitation coil was wound around each yoke. A Kepco BOP 100-4 M power amplifier supplied the coils plugged in series. For the magnetic excitation (H_{surf}) measurement, a linear Hall probe SS94A from Honeywell® was positioned tangentially to the surface of the tested sample. H_{surf} was measured on the left and right sides of the specimen (Fig. 3), and no difference was noticed, confirming the symmetry of the magnetic excitation. All tests were done at room temperature.

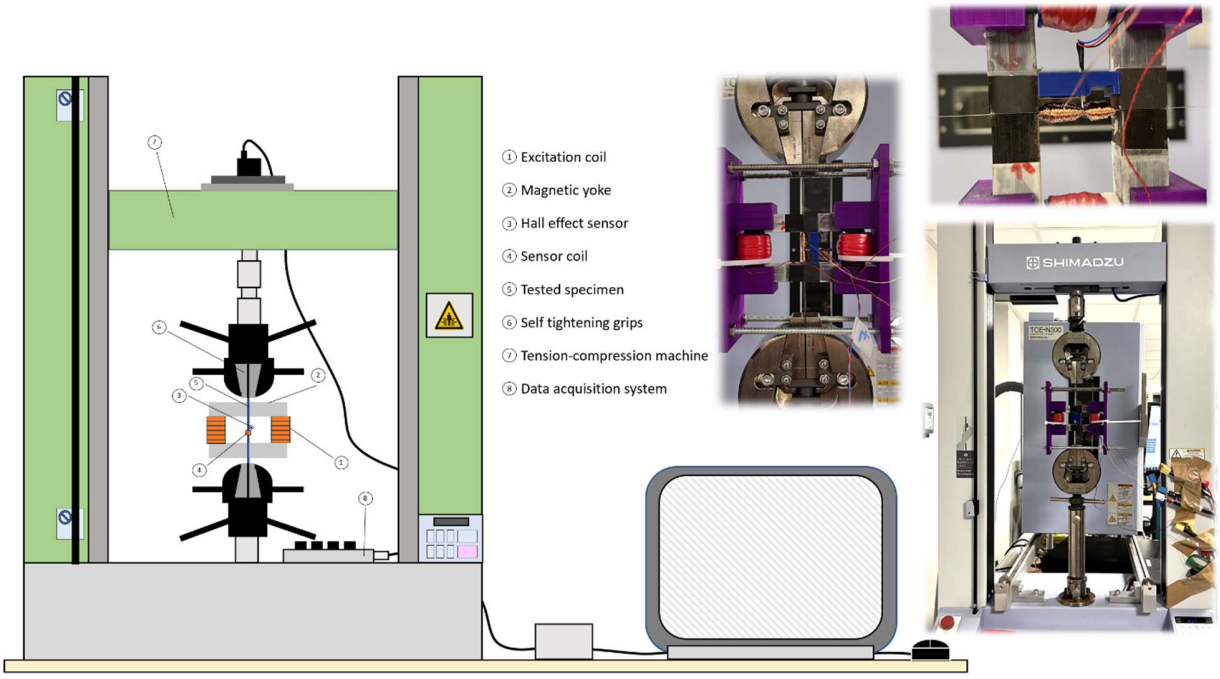

Fig. 3 – Experimental setup for the magnetic characterization under different tensile stress levels.

Fig. 3 shows a sketch of the experimental setup. An n = 300-turns pick-up coil was wrapped around the tested samples to measure the magnetic flux density B_a. B_a was obtained by numerical

integration of the electromotive force e(t) measured by the pick-up coils during the magnetization cycle. The tensile stress influence on the evolution of $B_a(H_{surf})$ hysteresis loops was evaluated for H_{surf} up to 5000 $A \cdot m^{-1}$. The considered tensile stress (denoted σ) range was 0-480 MPa. σ was intentionally set lower than $0.5 \cdot \sigma_c$ to avoid microplastic strains and keep the tested specimens in the elastic region. The absence of residual strain was confirmed by verifying the reproducibility of the B(H) curves after all tensile tests.

2.2) First experimental results

Tensile stress is expected to soften the magnetic behavior of the Permendur specimens as the magnetic moments gain a preferential direction (easy axis of magnetization direction) with the stress application (Fig. 4). However, applying a high magnetic field tends to align these moments in the applied field direction. The number of moments being constant, saturation magnetization is a material property, which will eventually be reached when H_{surf} is strong enough to compensate for the effect of stress. In the low-frequency range, softer magnetic behavior means higher permeability and lower coercivity. This behavior is well-known and has already been discussed in the literature (e.g., Fig. 2.34 in [49]). Fig. 4 depicts $B_a(H_{surf})$ hysteresis loops measured at different tensile stress levels. As expected, the material's permeability increases when the stress increases and the cycle is straightened.

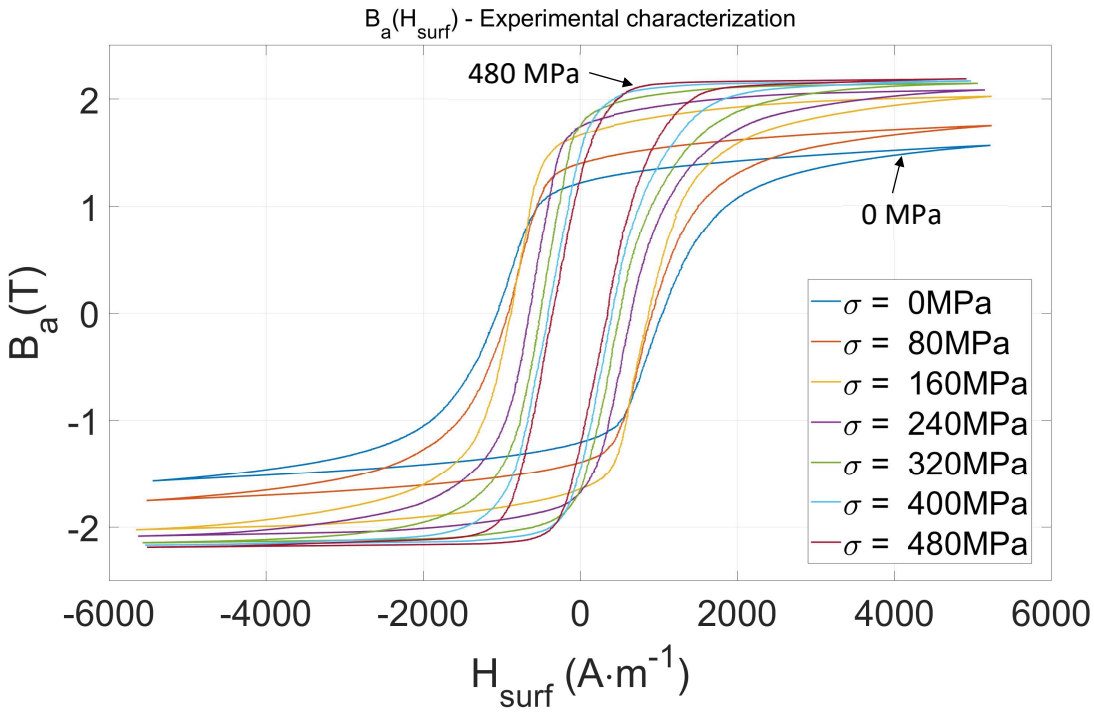

Fig. 4 – Fe-Co-V: $B_a(H_{surf})$ experimental hysteresis loops for different tensile stress levels.

III – Simulation method of the tensile-stress-dependent anhysteretic behavior

This section proposes an analytical method for simulating the Permendur sheets' magneto-mechanical response. The simulation method will be used afterward to assess the energy conversion performance and nonlinear effects (saturation, etc.). So far, multiple models have already been described in scientific literature to simulate the magneto-mechanical behavior of ferromagnetic materials. For instance, in [50][51], the multiaxial effect of stress is performed using an equivalent stress concept and uniaxial models. Even though this modeling approach can be successful for some configurations, it does not give a general description of the magneto-elastic behavior and can be inaccurate in some cases [52]. Another modeling approach is the multiscale approach, where local free energy at the domain scale is considered to get the macroscopic magneto-elastic behavior [53]. Another solution is obtained by defining a Helmholtz

free energy density, i.e., a function of five scalar invariants of the magneto-mechanical loading [54]. Here, the constitutive relationships of the material are obtained by minimizing this energy. All these methods are accurate and, most of the time, predictive but remain challenging to implement because of their computational cost, the required input data, and the delicate optimization process. In this study, where the experimental tests were limited to uniaxial tensile stress, we left them aside and opted for the simplified method described below.

As the ultimate goal of the present study lies in the energy conversion assessment in the framework of energy harvesting, the hysteresis property was not considered first. Indeed, only unipolar magnetization variations are induced by energy harvesting applications, limiting the hysteresis losses. This approach has already been proven effective since it allows obtaining analytical equations describing the energy conversion mechanism [55], thus facilitating the whole system optimization.

The simulation method was identified from uniaxial magneto-mechanical measurements. The objective was to obtain a fitting curve describing the behavior of anhysteretic curves reconstructed from measurements shown in Fig. 5 (experimental curves). These data are limited to the intermediate H_{surf} excitation level, and so is the simulation method. The anhysteretic curves obtained from experimental measurements are denoted as interpolated curve $B_{interp}(H_{surf})$ in Fig. 5 and are similar to sigmoid functions. Multiple analytical functions were tested, but Arctangent gave the best results. The resulting analytical expression, including the stress σ and the magnetic field H_{surf} dependency [56], yields:

$$B_{model}(H_{surf}, \sigma) = \left\{\left(1 + d \cdot \tanh(e \cdot \sigma)\right) \times \alpha\text{atan}[\beta \cdot H_{surf} \times \tanh(\kappa \cdot \sigma + 1)]\right\} \quad (1)$$

where α represents the maximal flux density at H_{surf} = 5000 A·m^{-1} (intermediate H_{surf}) and σ = 0. For very soft magnetic materials, where saturation is reached at very low magnetic excitation, α can be assimilated to $\mu_0 \cdot M_{sat}$, where M_{sat} is the magnetization saturation [56]. It is not the case for the Permendur, and both quantities must be distinguished. β is associated with the material's permeability in the Rayleigh region (i.e., in the low magnetic field amplitude).

The influence of stress σ on the magnetic flux density B_a is considered through two contributions:

- The first contribution consists in the modulation of parameter α by the hyperbolic (1 + d · tanh(e · σ)) function, where d and e are two material parameters: d is associated with the maximal flux density variation that tensile stress can induce, while e is its variation rate. We opted for a sigmoid shape function as the influence of stress is high in the low range of σ, then decreases and saturates for very high σ due to domains' reorganization.
- The second contribution comes from the modulation of parameter β by the tanh(κ · σ + 1) function. κ denotes how stress σ affects the magnetic permeability in the linear range and can also be seen as the manifestation of magnetostriction.

Finally, Eq. 1 parameters have been identified by performing a curve fitting from the preliminary experimental results, leading to Table 2.

Table 2: Simulation method parameters

Parameters	**Value**
α	1.02 T
β	0.002 A·m^{-1}
κ	0.0023×10^{-6} Pa^{-1}
D	0.464
E	0.0043×10^{-6} Pa^{-1}

Fig. 5 represents the experimental and the modeled curves for σ Є [0 – 480] MPa. Good agreement is observed between the anhysteretic curves derived from the experimental measurements and the model prediction. Fig. 6.a shows the flux density B_a level when H_{surf} is maximum. Again, both modeled and observed values follow the same trend. This figure confirms that according to the stress level, the material does not start to saturate for the same magnetic excitation.

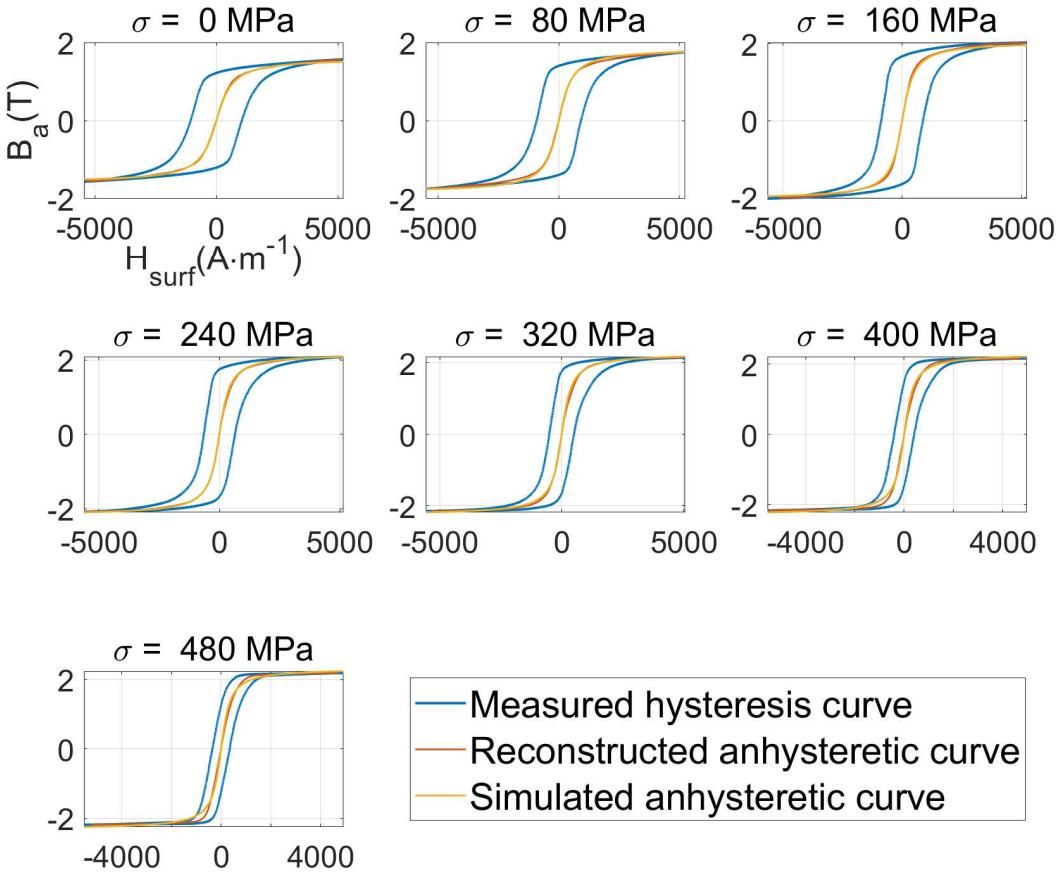

Fig. 5 – Comparisons between the experimental measurements, the reconstructed anhysteretic curves, and the simulation results.

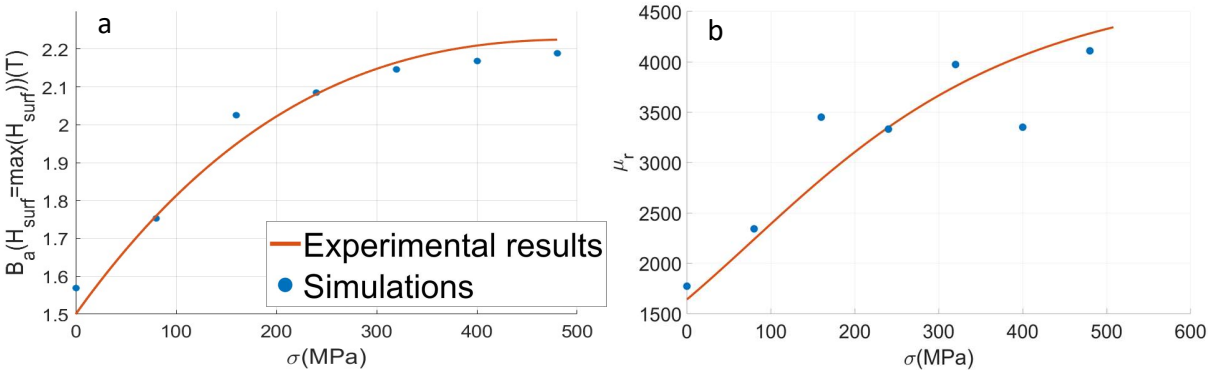

Fig. 6.a – Tensile stress dependency of the flux density at H_{surf} = 5000 A·m^{-1}. Fig. 6.b – Tensile stress dependency of the relative permeability in the low magnetic field region.

Fig. 6.b depicts the low-field permeability as a function of the applied stress. The permeability experimental value $\mu_{r\ exp}$ (Eq. 2) was obtained by measuring the slope of $B_{interp}(H_{surf})$ curve for H_{surf} = 0 A·m^{-1}:

$$\mu_{r\,exp}(\sigma) = \frac{\Delta B_{interp}(H,\sigma)}{\mu_0 \cdot \Delta H_{surf}} \quad (2)$$

The value of $\mu_{r\ sim}$ from the model was obtained by performing the first-order derivation of the arctangent function near zero:

$$\mu_{r\,sim}(\sigma) = \frac{\{(1+d\tanh(e\sigma))\times[\beta H_{surf}\times\tanh(\kappa\sigma+1)]\}}{\mu_0} \quad (3)$$

Fig. 6.b shows minor deviations between the fitted curve and the theoretical predictions, probably due to the simulation method. However, since we are working at a relatively high value of the magnetic field, meaning a relatively constant value of permeability, these deviations are considered negligible. It can be noted that, in the considered elastic stress region, low-field permeability increased with the tensile stress [56], which is consistent with the effect of stress on the magnetic moment, as previously stated.

IV – Ericsson cycle energy conversion

4.1) Estimation from the simulated anhysteretic curves

Experimental results (section II) showed an explicit dependency between the magnetic flux density B_a, the applied tensile stress σ, and the excitation field H_{surf}. This section investigates how these relations can be optimally exploited from the material electromechanical energy conversion point of view. More specifically, the converted energy (and available for extraction in a harvesting process) by the Permendur will be assessed, emphasizing the nonlinear effect of both the magnetic and mechanical excitations.

For simplicity, we considered only the purely magneto-mechanical conversion without the electromagnetic one, similar to other studies devoted to magneto-rheological elastomers [56]. It allows being independent from the number of turns of the coil for instance, hence giving a fair basis for material comparison.

The calculation of the ultimate converted energy during one cycle was considered to assess the energy conversion capability [57][58]. More precisely, this assessment was performed assuming a thermodynamic cycle close to the equivalent Ericsson cycle. An Ericsson cycle consists of two steps performed under constant stress and two other steps performed under constant magnetic excitation, as illustrated in Fig. 7.a and reported in [59][60]. The observation of Fig 7.b and 7.a, let us conclude with the possibility to reconstruct an Ericsson cycle from a pair of anhysteretic curves acquired at various stress levels. The constant stress steps follow the anhysteretic trajectories. The constant field steps represent vertical jumps from one anhysteretic curve to the other. The area enclosed by the resulting Ericsson cycle represents the converted energy density. The stress and no-stress anhysteretic curves merge beyond a threshold level in

the high field range, as depicted in Fig 7.b. Application of larger fields will not modify the energy density beyond this level, and the resulting Ericsson cycle area can be regarded as the material's ultimate energy density. More specifically, during the first step (1 – 2), the magnetic excitation field was increased to a value H_M while the stress was kept constant at σ_{max}. During the second step (2 – 3), the excitation field H_M was kept constant, and the stress on the material was reduced until σ_{min}. The magnetic induction field decreases in this stage, as shown in Fig. 8 of [56]. During the third step (3 – 4), the excitation field decreased to zero while the stress remained constant at σ_{min}.

The closed loop area in the $B_a(H_{surf})$ diagram (cycle 1 - 2 - 3 - 4 in our case) corresponds to the energy converted from mechanical to magnetic energy. The maximum potential extractable energy between σ [0 - 480 MPa] and H_{surf} [0 - 5500 $A \cdot m^{-1}$] was determined, as shown in Fig. 7.b.

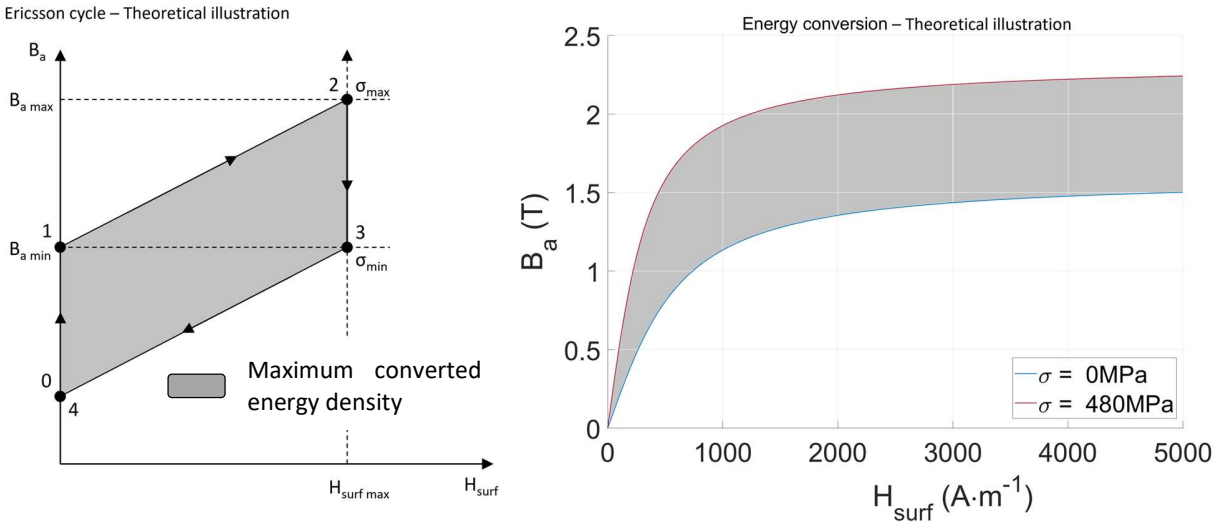

Fig. 7.a – Illustration of the thermodynamic Ericsson cycles used to estimate the energy conversion capability. Fig. 7.b Extractable energy vs. H_{surf} and for different tensile stress levels.

For a single cycle, the energy W is given by:

$$-W = \int H_{surf} \cdot dB_{loop} \quad (4)$$

$$W = \int_0^{H_M} -\Delta B_a \cdot dH_{surf} \quad (5)$$

Eq. 4 and 5 are the ferromagnetic dual expression of Eq. 2 in [61] and Eq. 1 in [62], where the Ericsson cycle principle is applied to a ferroelectric conversion. Eq. 5 leads to the graph shown in Fig. 8. Beyond a threshold of approximately H_{surf} = 250 A·m^{-1}, and for all stress levels, the converted energy follows a quasi-linear trajectory as the magnetic flux density does not vary significantly for a given stress level. The relatively weak difference between both extreme values of stress is noteworthy.

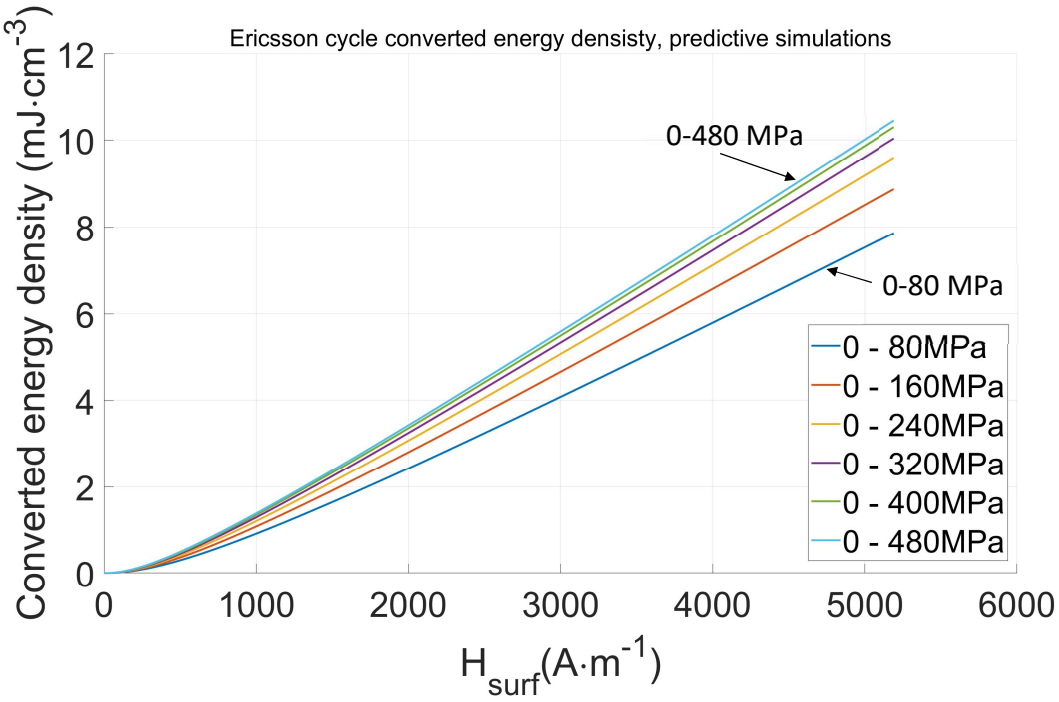

Fig. 8 – Ericsson cycle converted energy density vs. H_{surf}, based on the reconstructed anhysteretic curves and for different stress levels.

Table 3 summarizes the maximum converted energy obtained with the anhysteretic curves method, considering a magnetic excitation field of max(H_{surf}) = 5500 A·m^{-1} and different stress levels. As observed in Fig. 8, Table 3 confirms the relatively weak influence of the stress level beyond 240 MPa.

Table 3: Maximum Ericsson cycle converted energy density for different stress levels, as obtained with the reconstructed anhysteretic curve and the hysteresis loop methods.

σ (MPa)	Max. energy density – anhysteretic method (mJ·cm^{-3})	Max. energy density - hysteresis loop method (mJ·cm^{-3})
0-80	7.86	1.37
0-160	8.89	2.59
0-240	9.6	2.95
0-320	10.04	3.28
0-400	10.31	3.41
0-480	10.45	3. 52

4.2) Direct estimation from the $B_a(H_{surf})$ hysteresis cycles

The previous section described a method to estimate the Ericsson cycle energy densities using the anhysteretic curves reconstructed from $B_a(H_{surf})$ cycles under low and high stresses, respectively (1 – 2 – 3 – 4 cycle in Fig. 7.a). But this estimation is inaccurate as the hysteresis losses are not considered.

This section proposes a further step to truly evaluate the energy conversion through an alternative semi-empirical estimation (Fig. 9). The alternative method relies on the Ericsson cycle formed with the two descending curves of the hysteresis cycles measured with and without stress (B_1 – B_r – C – D, red dashed in Fig. 9). However, this cycle remains imprecise as the hysteresis losses are not considered. Because of the hysteresis, the real experimental Ericsson cycle trajectory undergoes a first-order reversal curve between B_r and C. Therefore, in the final stage, the ascending curve of the $B_a(H_{surf})$ hysteresis loop under high tensile stress, denoted $f(H_{surf})$, is shifted upward to become $g(H_{surf})$ and is considered equivalent to a first-order reversal curve [63]. $f(H_{surf})$ is not expressed analytically, and the experimental observations in a data file form

are used instead. Hence, the estimated Ericsson cycle became the B_1 – $g(H_{surf})$ – C – D – B_1 cycle (Fig. 9), and $g(H_{surf})$ is calculated from $f(H_{surf})$ according to:

$$g(H_{surf}) = f(H_{surf}) \cdot \frac{B_2 - B_1}{B_2 - B_3} + B_1 - B_3 \cdot \frac{B_2 - B_1}{B_2 - B_3} \quad (6)$$

This equation has not been derived from any other equation and was proposed to reproduce closely a first-order reversal curve shape.

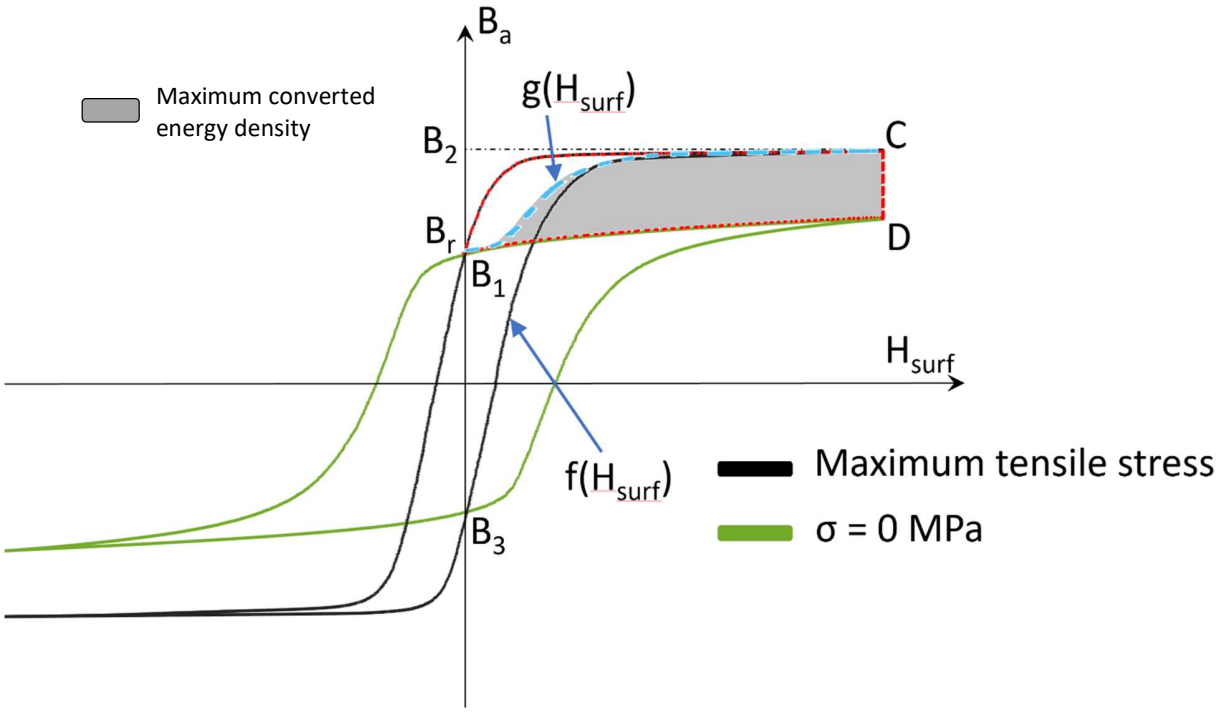

Fig. 9 – $B_a(H_{surf})$ hysteresis loops at σ = 0 MPa and high tensile stress. Illustration of the B_1- $g(H_{surf})$ -C-D-B_1 Ericsson cycle as obtained from these curves.

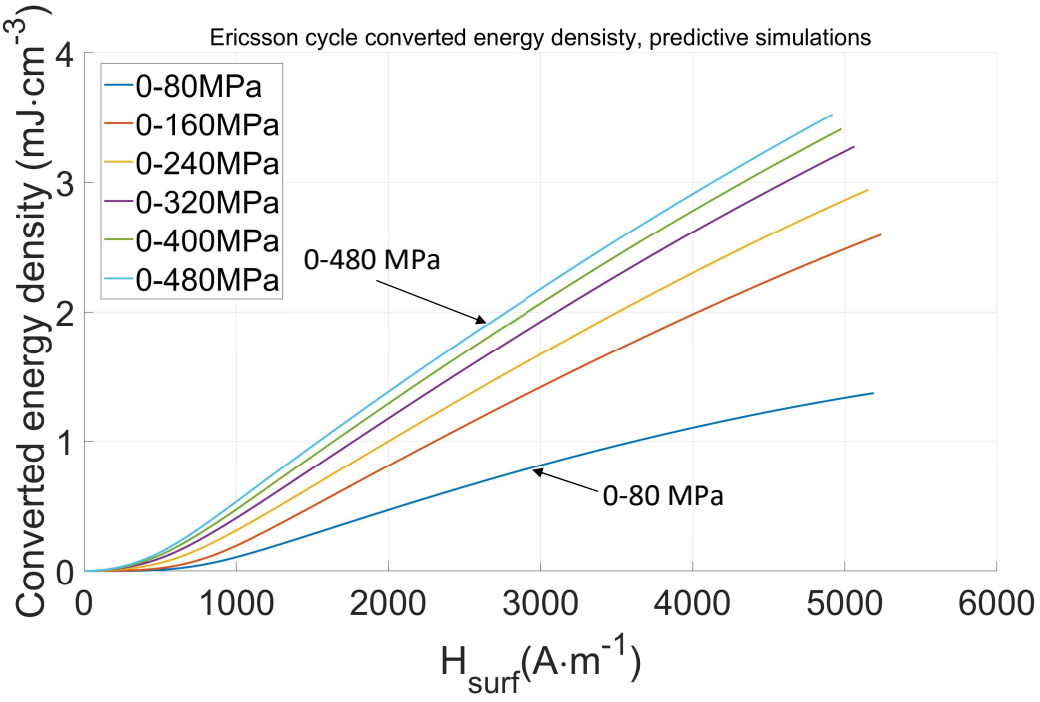

Fig. 10 – Ericsson cycle converted energy density vs. H_{surf}, based on the hysteresis loop measured at different stress levels.

The semi-empirical estimation method shows a larger stress influence. Beyond a threshold level close to 300 MPa, a pseudo-saturation is reached, and the variation from one stress level to the other is less significant. Comparing Fig. 8 and 10 allows for highlighting the hysteresis loss impact on the level of converted energy. The dependency is especially remarkable under low-stress levels, dividing the amount of harvested energy by more than 50% when σ is lower than σ = 160 MPa. Table 3 establishes a comparison between the maximum energy converted between the anhysteretic and the hysteresis loop methods ($max(H_{surf})$ = 5500 $A{\cdot}m^{-1}$). As expected, the hysteresis loop methods energy predictions are much lower than the anhysteretic curve ones. The difference in shape between the reconstructed Ericsson cycle (Fig. 9) and the experimental one later shown in this manuscript is worth noting. This difference is due to the 1 – 2 step

(increase of the stress step), which is supposed to be under no field variation, which is definitively not the case in the reconstructed cycle.

V – Experimental validation of the Ericsson cycle

In the final stage of this study, practical Ericsson cycles were implemented and measured to validate the feasibility of energy conversion and to confirm the energy level predictions. The experimental setup described in Section 2 is versatile and allows magnetic and mechanical stress excitation to be imposed simultaneously. In the case of the Ericsson cycle, the magnetic field and mechanical stress chronograms are depicted in Fig. 11. Working points 1 to 4 are reported in Fig. 12 for illustration.

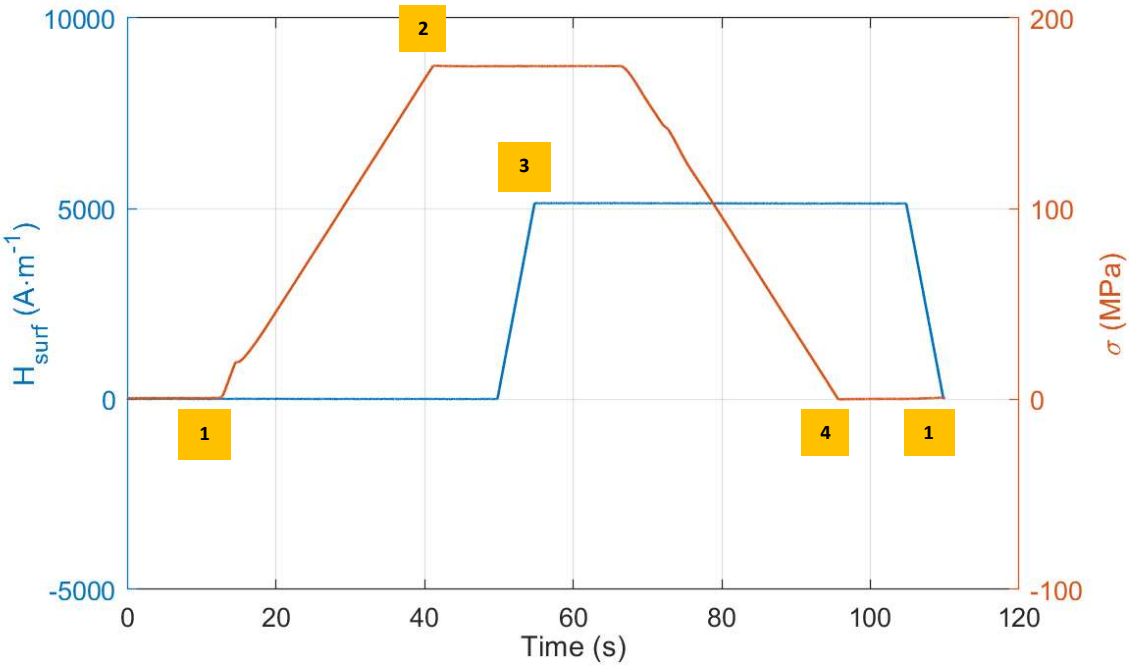

Fig. 11 – Experimental Ericsson cycle magnetic field H_{surf} and stress σ chronograms.

Fig. 12 shows the resulting Ericsson cycle (in terms of relative values, as the initial magnetic state of the tested specimen was unknown), and Fig. 13 shows the evolution of the harvested energy density for σ = 175 MPa. It is worth mentioning that the tensile stress level was limited to avoid drifts observed beyond σ = 175 MPa, yielding open Ericsson cycles.

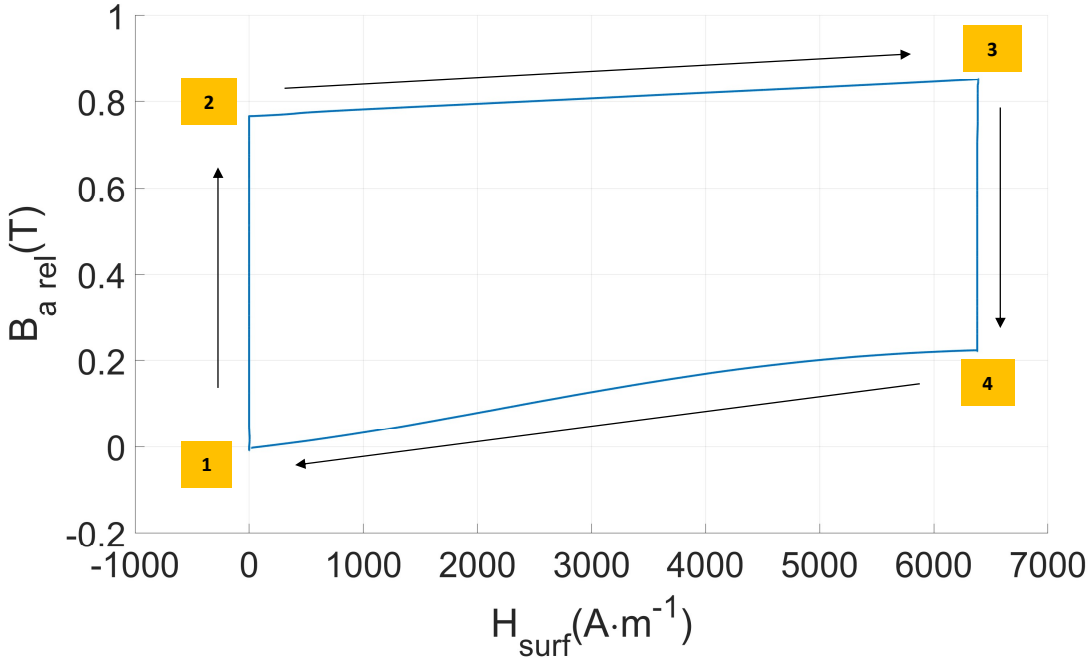

Fig. 12 – Experimental Ericsson cycle (max(H_{surf}) = 6400 A·m^{-1}, σ = 175 MPa).

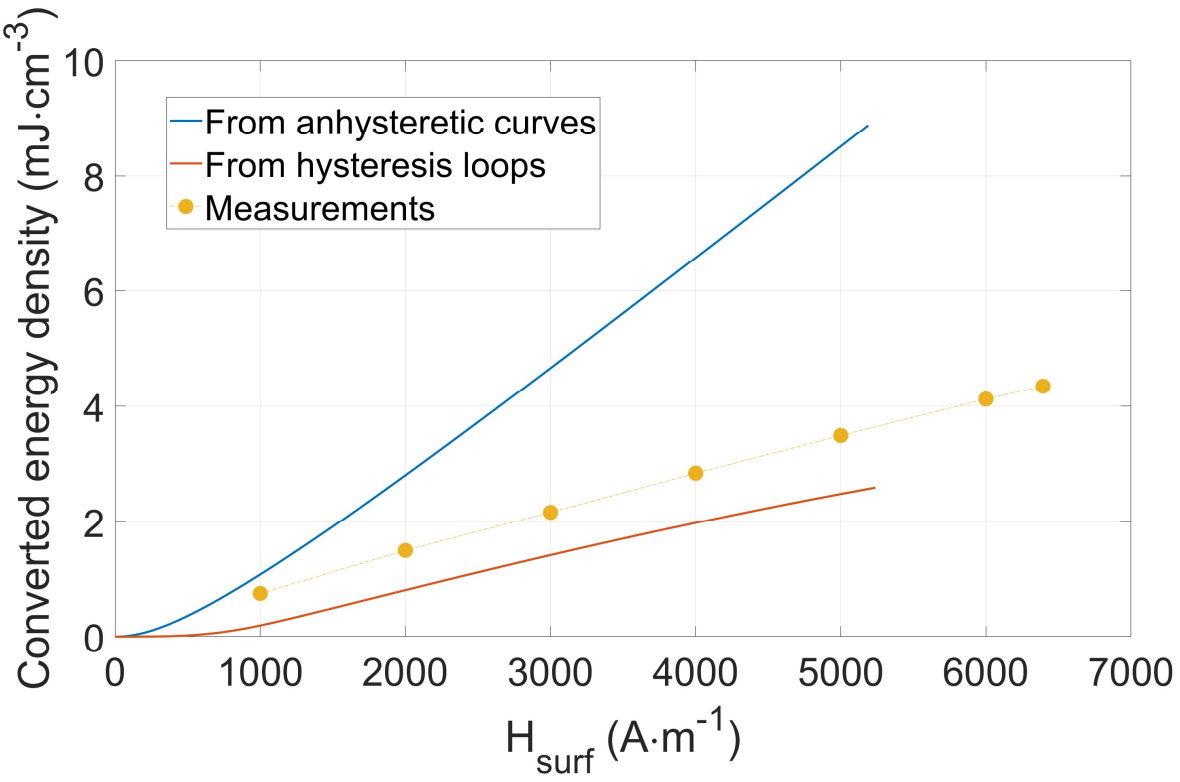

Fig. 13 – Converted energy density vs. H_{surf}, comparisons predictions/measurement (σ = 175 MPa)

As forecasted, the semi-empirical estimation from the hysteresis loops is more accurate in its prediction than the anhysteretic ones. More than 4 mJ·cm^{-3} was reached, and it seems reasonable to anticipate up to two times this amount in higher stress conditions. The overestimation of the anhysteretic method is undoubtedly due to the absence of losses and remnant magnetization considerations. The underestimation of the hysteresis loop method can be attributed to the underevaluation of the demagnetization effect during the Ericsson cycle process.

While it may seem that focusing on a single mechanical stress level limits the comprehensiveness of our study, it is imperative to emphasize that at σ = 175 MPa, the stress-induced effects on the Ericsson cycle are already quite remarkable. This stress level is substantial

enough to impact the cycle significantly, and the potential effect of higher stress levels is anticipated to be marginal.

One of the limits of the magnetostrictive energy harvester is the need for significant stress variations and high magnetic field bias. But to overcome it, one can work on the optimum magnetic field value at the maximum magnetoelastic coefficient. Recently, a study [35] verified this on a magnetostrictive Metglas material where these ideal working conditions were obtained at a low magnetic excitation zone compared to Terfenol and Galfenol, which usually require bias fields higher than 20 $kA{\cdot}m^{-1}$ (Table 1 of [35]). For Metglas 2605SA1, a magnetoelastic coefficient of nearly 15 $mT{\cdot}MPa^{-1}$ was obtained at 100 $kA{\cdot}m^{-1}$, illustrating a realistic implementation of magnetostrictive harvesters.

VI – Conclusions

Low-frequency mechanical energy conversion based on tensile stress application to magnetostrictive Permendur material was studied in this work. Permendur is highly magnetostrictive, low-cost, and abundant, yielding an ideal candidate for energy conversion applications. Tensile stress tests were performed as a first step and used as experimental bases for establishing theoretical tools. A simulation method was proposed based on an analytical function describing the effects of stress and magnetic field on the anhysteretic magnetization curve. The formula requires only two material parameters (saturation field and permeability). The obtained simulation results were proved to be in good agreement with experimental ones. Then, using Ericsson cycles, the energy conversion was predicted from the calculated anhysteretic curves. A maximum of converted magnetic energy was forecasted to be equal to

10.45 mJ·cm^{-3} under a tensile stress of σ = 480 MPa and a magnetic excitation of 5.5 kA·m^{-1}. Yet, Permendur coercivity is not so small and will result in core losses that might reduce the conversion efficiency. Still, when the stress is tensile, the comparison with recent results on a very soft Metglas material [35] shows that the influence of coercivity is minor. The effect of the stress when saturation starts is much more influential, though. Hence, a relevant solution consists of a permanent magnet bias field to shift the working condition in the saturation zone where hysteresis is significantly reduced, and the stress influence is still substantial.

Then, to consider hysteresis, another experimental estimation of the converted energy density was proposed based on hysteresis loops. An energy density of up to 3.52 mJ·cm^{-3} was obtained in the same conditions. This value appears to be excessive compared to the Galfenol and Terfenol-D results depicted in Table 1, but the experimental conditions are entirely different (σ < 10 MPa in [32], for example), making the comparison delicate. This value can also be compared to other energy conversion processes, such as piezoelectric conversion, where the energy density may reach hundreds of mJ·cm^{-3} [8]. The difference in the order of magnitude may be attributed to the relatively high electrostrictive strain of ferroelectrics that may reach thousands of ppm or even close to 1% in some compounds [64].

Then, experimental Ericsson cycles were experimentally assessed to prove the feasibility and confirm the energy level predictions. The comparison between the predictive methods and the experimental tests showed an overestimation of the model based on the anhysteretic curve, especially in the high field range. The prediction based on the major hysteresis loops was much more accurate, especially in terms of the slope of the converted energy vs. magnetic field curve. The predicted value of converted energy as a function of the excitation field amplitude slightly

underestimated the experimental result (4 mJ·cm^{-3}) by a constant term, which can be attributed to the level of mechanical stress (slightly lower in the simulation: σ = 160 MPa vs. 175 MPa) or an overestimation of the hysteresis losses.

Many perspectives can be listed for this work, including:

- the test of predictive methods under compressive stress,
- the consideration of different stress levels,
- the investigation of the dynamic behavior,
- the development of a real energy harvester and assess the material effect on the next stages and conversely,
- to take advantage of the material nonlinearity to design efficient energy harvesters (structure and electrical interface).

Data availability statement: Data available on request due to privacy/ethical restrictions.

References

[1] Zhang, S. and Zhang, H., 2012, August. A review of wireless sensor networks and its applications. In *2012 IEEE international conference on automation and logistics* (pp. 386-389). IEEE.

[2] Ng, I.C. and Wakenshaw, S.Y., 2017. The Internet-of-Things: Review and research directions. *International Journal of Research in Marketing*, *34*(1), pp.3-21.

[3] Wang, L. and Yuan, F.G., 2008. Vibration energy harvesting by magnetostrictive material. Smart Materials and Structures, 17(4), p.045009.

[4] Sachan, V.K., Imam, S.A. and Beg, M.T., 2012. Energy-efficient communication methods in wireless sensor networks: A critical review. International Journal of Computer Applications, 39(17), pp.35-48.

[5] Deng, Z. and Dapino, M.J., 2017. Review of magnetostrictive vibration energy harvesters. *Smart Materials and Structures*, *26*(10), p.103001.

[6] Selvan, K.V. and Ali, M.S.M., 2016. Micro-scale energy harvesting devices: Review of methodological performances in the last decade. *Renewable and Sustainable Energy Reviews*, *54*, pp.1035-1047.

[7] Krikke, J., 2005. Sunrise for energy harvesting products. *IEEE Pervasive Computing*, *4*(1), pp.4-5..

[8] Tung, N.T., Taxil, G., Nguyen, H.H., Ducharne, B., Lallart, M., Lefeuvre, E., Kuwano, H. and Sebald, G., 2022. Ultimate electromechanical energy conversion performance and energy storage capacity of ferroelectric materials under high excitation levels. *Applied Energy*, *326*, p.119984.

[9] Mizukawa, Y., Ahmed, U., Zucca, M., Blažević, D. and Rasilo, P., 2022. Small-signal modeling and optimal operating condition of magnetostrictive energy harvester. *Journal of Magnetism and Magnetic Materials*, *547*, p.168819.

[10] Anton, S.R. and Sodano, H.A., 2007. A review of power harvesting using piezoelectric materials (2003–2006). *Smart materials and Structures*, *16*(3), p.R1.

[11] Dapino, M.J., 2002. Magnetostrictive materials. *Encyclopedia of Smart Materials*, *2*, pp.600-620.

[12] Dey, S., Roy, D., Patra, S. and Santra, T., 2019. Performance of a modified magnetostrictive energy harvester in mechanical vibration. *Heliyon*, *5*(1).

[13] Zhao, X. and Lord, D.G., 2006. Application of the Villari effect to electric power harvesting. *Journal of applied physics*, *99*(8).

[14] Dai, X., Wen, Y., Li, P., Yang, J. and Li, M., 2011. Energy harvesting from mechanical vibrations using multiple magnetostrictive/piezoelectric composite transducers. *Sensors and Actuators A: Physical*, *166*(1), pp.94-101.

[15] Liu, H., Cao, C., Sun, X., Zhao, L. and Cong, C., 2020. Magnetostrictive iron–gallium alloy harvester with efficient two-mode AC–DC converting technology for effective vibration energy harvesting. *AIP Advances*, *10*(11).

[16] Mohanty, A., Parida, S., Behera, R.K. and Roy, T., 2019. Vibration energy harvesting: A review. *Journal of Advanced Dielectrics*, *9*(04), p.1930001.

[17] Clemente, C.S., Mahgoub, A., Davino, D. and Visone, C., 2017. Multiphysics circuit of a magnetostrictive energy harvesting device. *Journal of Intelligent Material Systems and Structures*, *28*(17), pp.2317-2330.

[18] Zucca, M., Bottauscio, O., Beatrice, C., Hadadian, A., Fiorillo, F. and Martino, L., 2014. A study on energy harvesting by amorphous strips. *IEEE Transactions on Magnetics*, *50*(11), pp.1-4.

[19] Kai, Y., Tsuchida, Y., Todaka, T. and Enokizono, M., 2014. Influence of biaxial stress on vector magnetic properties and 2-D magnetostriction of a nonoriented electrical steel sheet under alternating magnetic flux conditions. *IEEE Transactions on magnetics*, *50*(4), pp.1-4.

[20] Anderson, P.I., Moses, A.J. and Stanbury, H.J., 2007. Assessment of the stress sensitivity of magnetostriction in grain-oriented silicon steel. *IEEE transactions on magnetics*, *43*(8), pp.3467-3476.

[21] Rekik, M., Hubert, O. and Daniel, L., 2014. Influence of a multiaxial stress on the reversible and irreversible magnetic behaviour of a 3% Si-Fe alloy. *International Journal of Applied Electromagnetics and Mechanics*, *44*(3-4), pp.301-315.

[22] Perevertov, O., 2017. Influence of the applied elastic tensile and compressive stress on the hysteresis curves of Fe-3% Si non-oriented steel. *Journal of Magnetism and Magnetic Materials*, *428*, pp.223-228.

[23] Perevertov, O., Thielsch, J. and Schäfer, R., 2015. Effect of applied tensile stress on the hysteresis curve and magnetic domain structure of grain-oriented transverse Fe-3% Si steel. *Journal of Magnetism and Magnetic Materials*, *385*, pp.358-367.

[24] Hubert, A. and Schäfer, R., 2008. *Magnetic domains: the analysis of magnetic microstructures*. Springer Science & Business Media.

[25] Dapino, M.J., Smith, R.C., Calkins, F.T. and Flatau, A.B., 2002. A coupled magnetomechanical model for magnetostrictive transducers and its application to Villari-effect sensors. *Journal of intelligent material systems and structures*, *13*(11), pp.737-747.

[26] Ahmed, U., Aydin, U., Daniel, L. and Rasilo, P., 2020. 3-D magneto-mechanical finite element analysis of Galfenol-based energy harvester using an equivalent stress model. *IEEE Transactions on Magnetics*, *57*(2), pp.1-5.

[27] Palumbo, S., Rasilo, P. and Zucca, M., 2019. Experimental investigation on a Fe-Ga close yoke vibrational harvester by matching magnetic and mechanical biases. *Journal of Magnetism and Magnetic Materials*, *469*, pp.354-363.

[28] Davino, D., Giustiniani, A., Visone, C. and Zamboni, W., 2011. Stress-induced eddy currents in magnetostrictive energy harvesting devices. *IEEE transactions on magnetics*, *48*(1), pp.18-25.

[29] Wang, L. and Yuan, F.G., 2008. Vibration energy harvesting by magnetostrictive material. *Smart Materials and Structures*, *17*(4), p.045009.

[30] Park, Y.W., Kang, H.S. and Wereley, N.M., 2014. Conceptual design of rotary magnetostrictive energy harvester. *Journal of Applied Physics*, *115*(17).

[31] Davino, D., Giustiniani, A., Visone, C. and Adly, A.A., 2012. Energy harvesting tests with Galfenol at variable magneto-mechanical conditions. *IEEE Transactions on Magnetics*, *48*(11), pp.3096-3099.

[32] Zucca, M., Hadadian, A. and Bottauscio, O., 2015. Quantities affecting the behavior of vibrational magnetostrictive transducers. *IEEE Transactions on Magnetics*, *51*(1), pp.1-4.

[33] Yamaura, S.I., Nakajima, T., Kamata, Y., Sasaki, T. and Sekiguchi, T., 2020. Production of vibration energy harvester with impact-sliding structure using magnetostrictive Fe-Co-V alloy rod. *Journal of Magnetism and Magnetic Materials*, *514*, p.167260.

[34] Kita, S., Ueno, T. and Yamada, S., 2015. Improvement of force factor of magnetostrictive vibration power generator for high efficiency. *Journal of Applied Physics*, *117*(17).

[35] Liu, Y., Ducharne, B., Sebald, G., Makihara, K. and Lallart, M., 2023. Investigation of Energy Harvesting Capabilities of Metglas 2605SA1. *Applied Sciences*, *13*(6), p.3477.

[36] Berbyuk, V., 2013, April. Vibration energy harvesting using Galfenol-based transducer. In *Active and Passive Smart Structures and Integrated Systems 2013* (Vol. 8688, pp. 429-440). SPIE.

[37] Staley, M.E. and Flatau, A.B., 2005, May. Characterization of energy harvesting potential of Terfenol-D and Galfenol. In *Smart Structures and Materials 2005: Smart Structures and Integrated Systems* (Vol. 5764, pp. 630-640). SPIE.

[38] Dai, X., Wen, Y., Li, P., Yang, J. and Zhang, G., 2009. Modeling, characterization and fabrication of vibration energy harvester using Terfenol-D/PZT/Terfenol-D composite transducer. *Sensors and Actuators A: Physical*, *156*(2), pp.350-358.

[39] Zhu, Y., Zu, J.W. and Guo, L., 2012. A magnetoelectric generator for energy harvesting from the vibration of magnetic levitation. *IEEE Transactions on magnetics*, *48*(11), pp.3344-3347.

[40] Zhao, X. and Lord, D.G., 2006. Application of the Villari effect to electric power harvesting. *Journal of applied physics*, *99*(8).

[41] Abramovich, H., 2021. *Intelligent materials and structures*. Walter de Gruyter GmbH & Co KG.

[42] Lafont, T., Gimeno, L., Delamare, J., Lebedev, G.A., Zakharov, D.I., Viala, B., Cugat, O., Galopin, N., Garbuio, L. and Geoffroy, O., 2012. Magnetostrictive–piezoelectric composite structures for energy harvesting. *Journal of Micromechanics and Microengineering*, *22*(9), p.094009.

[43] Clark, A.E., Wun-Fogle, M., Restorff, J.B. and Lograsso, T.A., 2002. Magnetostrictive properties of Galfenol alloys under compressive stress. *Materials transactions*, *43*(5), pp.881-886..

[44] Deng, Z. and Dapino, M.J., 2015, April. Multiphysics modeling and design of Galfenol-based unimorph harvesters. In *Industrial and Commercial Applications of Smart Structures Technologies 2015* (Vol. 9433, pp. 74-83). SPIE.

[45] Daniel, L. and Domenjoud, M., 2021. Anhysteretic magneto-elastic behaviour of Terfenol-D: Experiments, multiscale modelling and analytical formulas. *Materials*, *14*(18), p.5165.

[46] Fiorillo, F., 2010. Magnetic materials for electrical applications: A Review. *INRIM Istituto Nazionale di Ricerca Metrologica, Tech. Rep. TR 13/2010*.

[47] Fagan, P., Ducharne, B., Daniel, L. and Skarlatos, A., 2021. Multiscale modelling of the magnetic Barkhausen noise energy cycles. *Journal of Magnetism and Magnetic Materials*, *517*, p.167395.

[48] Toutsop, B., Ducharne, B., Lallart, M., Morel, L. and Tsafack, P., 2022. Characterization of Tensile Stress-Dependent Directional Magnetic Incremental Permeability in Iron-Cobalt Magnetic Sheet: Towards Internal Stress Estimation through Non-Destructive Testing. *Sensors*, *22*(16), p.6296.

[49] Rekik, M., 2014. *Mesure et modélisation du comportement magnéto-mécanique dissipatif des matériaux ferromagnétiques à haute limite élastique sous chargement multiaxial* (Doctoral dissertation, École normale supérieure de Cachan-ENS Cachan).

[50] Daniel, L. and Hubert, O., 2009. An equivalent stress for the influence of multiaxial stress on the magnetic behavior. *Journal of Applied Physics*, *105*(7).

[51] Hubert, O. and Daniel, L., 2011. Energetical and multiscale approaches for the definition of an equivalent stress for magneto-elastic couplings. *Journal of Magnetism and Magnetic Materials*, *323*(13), pp.1766-1781.

[52] Aydin, U., Rasilo, P., Martin, F., Belahcen, A., Daniel, L. and Arkkio, A., 2020. Modeling of multi-axial stress dependent iron losses in electrical steel sheets. *Journal of Magnetism and Magnetic Materials*, *504*, p.166612.

[53] Fagan, P., Ducharne, B., Daniel, L., Skarlatos, A., Domenjoud, M. and Reboud, C., 2022. Effect of stress on the magnetic Barkhausen noise energy cycles: A route for stress evaluation in ferromagnetic materials. *Materials Science and Engineering: B*, *278*, p.115650.

[54] Clemente, C.S., Mahgoub, A., Davino, D. and Visone, C., 2017. Multiphysics circuit of a magnetostrictive energy harvesting device. *Journal of Intelligent Material Systems and Structures*, *28*(17), pp.2317-2330.

[55] Agayan, V., 1996. Thermodynamic model of ideal magnetostriction. *Physica Scripta*, *54*(5), p.514.

[56] Sebald, G., Nakano, M., Lallart, M., Tian, T., Diguet, G. and Cavaille, J.Y., 2017. Energy conversion in magneto-rheological elastomers. *Science and Technology of advanced MaTerialS*, *18*(1), pp.766-778.

[57] Hristoforou, E., Ktena, A., Vourna, P. and Argiris, K., 2018. Dependence of magnetic permeability on residual stresses in alloyed steels. *AIP Advances*, *8*(4).

[58] Tung, N.T., Taxil, G., Nguyen, H.H., Ducharne, B., Lallart, M., Lefeuvre, E., Kuwano, H. and Sebald, G., 2022. Ultimate electromechanical energy conversion performance and energy storage capacity of ferroelectric materials under high excitation levels. Applied Energy, 326, p.119984.

[59] Sebald, G., Pruvost, S. and Guyomar, D., 2007. Energy harvesting based on Ericsson pyroelectric cycles in a relaxor ferroelectric ceramic. *Smart Materials and Structures*, *17*(1), p.015012.

[60] Zhang, B., Ducharne, B., Gupta, B., Sebald, G., Guyomar, D. and Gao, J., 2018. Experimental sea wave energy extractor based on piezoelectric Ericsson cycles. *Journal of Intelligent Material Systems and Structures*, *29*(6), pp.1102-1112.

[61] Unruan, M., Unruan, S., Inkong, Y. and Yimnirun, R., 2019. Estimation of energy density of PMN-PT ceramics utilizing mechanical stress. *Integrated Ferroelectrics*, *195*(1), pp.39-45.

[62] Patel, S., Chauhan, A. and Vaish, R., 2014. Enhanced energy harvesting in commercial ferroelectric materials. *Materials Research Express*, *1*(2), p.025504.

[63] Goh, Y. and Jeon, S., 2018. First-order reversal curve diagrams for characterizing ferroelectricity of Hf0. 5Zr0. 5O2 films grown at different rates. *Journal of Vacuum Science & Technology B*, *36*(5).

[64] Park, S.E. and Shrout, T.R., 1997. Ultrahigh strain and piezoelectric behavior in relaxor based ferroelectric single crystals. *Journal of applied physics*, *82*(4), pp.1804-1811.